5-1-2009

Inducer responses of BenM, a LysR-type transcriptional regulator from Acinetobacter baylyi ADP1.

Sarah H Craven

Obidimma Ezezika

Sandra Haddad

Ruth A Hall

Cory Momany

See next page for additional authors

Molecular Microbiology (2009) 72(4), 881–894 ■
doi:10.1111/j.1365-2958.2009.06686.x
First published online 16 April 2009

Inducer responses of BenM, a LysR-type transcriptional regulator from *Acinetobacter baylyi* ADP1

Sarah H. Craven,[1] Obidimma C. Ezezika,[1†] Sandra Haddad,[1] Ruth A. Hall,[1‡] Cory Momany[2] and Ellen L. Neidle[1*]
[1]*Departments of Microbiology and* [2]*Pharmaceutical and Biomedical Sciences, University of Georgia, Athens, GA 30602-2605, USA.*

Summary

BenM and CatM control transcription of a complex regulon for aromatic compound degradation. These *Acinetobacter baylyi* paralogues belong to the largest family of prokaryotic transcriptional regulators, the LysR-type proteins. Whereas BenM activates transcription synergistically in response to two effectors, benzoate and *cis,cis*-muconate, CatM responds only to *cis,cis*-muconate. Here, site-directed mutagenesis was used to determine the physiological significance of an unexpected benzoate-binding pocket in BenM discovered during structural studies. Residues in BenM were changed to match those of CatM in this hydrophobic pocket. Two BenM residues, R160 and Y293, were found to mediate the response to benzoate. Additionally, alteration of these residues caused benzoate to inhibit activation by *cis,cis*-muconate, positioned in a separate primary effector-binding site of BenM. The location of the primary site, in an interdomain cleft, is conserved in diverse LysR-type regulators. To improve understanding of this important family, additional regulatory mutants were analysed. The atomic-level structures were characterized of the effector-binding domains of variants that do not require inducers for activation, CatM(R156H) and BenM(R156H,T157S). These structures clearly resemble those of the wild-type proteins in their activated muconate-bound complexes. Amino acid replacements that enable activation without effectors reside at protein interfaces that may impact transcription through effects on oligomerization.

Accepted 27 March, 2009. *For correspondence. E-mail eneidle@uga.edu; Tel. (+1) 706 542 2852; Fax (+1) 706 542 2674. Present addresses: †McLaughlin-Rotman Centre for Global Health, Toronto, Canada; ‡Department of Microbiology, University of Washington, Seattle, WA 98195, USA.

Introduction

Nearly 20% of all transcriptional regulators identified by bacterial genome analysis are LysR-type transcriptional regulators (LTTRs), the largest regulatory family in prokaryotes (Pareja *et al.*, 2006). Despite this prevalence, the molecular basis of effector-induced activation by LTTRs remains unclear. Aggregation problems impede structural studies, and there are only two known atomic-level structures of LTTRs bound to their cognate inducers (Ezezika *et al.*, 2007a). These structures encompass the effector-binding domains (EBDs) of CatM and BenM, two similar LTTRs that control benzoate degradation in the soil bacterium *Acinetobacter baylyi* ADP1 (Fig. 1) (Romero-Arroyo *et al.*, 1995; Collier *et al.*, 1998). BenM- and CatM-EBD both bind an inducer in an interdomain cleft. Surprisingly, a secondary effector-binding site was discovered in a hydrophobic pocket of BenM-EBD. In the current investigation, the physiological significance of this discovery was tested. LTTR–inducer interactions were explored further by characterizing mutants with atypical responses to effectors.

In LTTRs, the N-terminal DNA-binding domain is linked to the EBD, which extends to the C-terminus and is composed of two subdomains. The characterized structures of one full-length LTTR and the regulatory regions of several others demonstrate that the protein fold of the EBD is essentially that of a periplasmic-binding protein (Quiocho and Ledvina, 1996; Choi *et al.*, 2001; Muraoka *et al.*, 2003; Smirnova *et al.*, 2004; Stec *et al.*, 2006). The structural conservation in this domain is remarkable in light of the sequence variability in different LTTRs. For example, the structurally similar EBDs of BenM and CysB share only 12% sequence identity (Tyrrell *et al.*, 1997; Verschueren *et al.*, 1999). Consistent with the typical role of the EBD in binding a low-molecular-weight inducer, LTTRs that respond to the same or similar compounds share a higher degree of sequence similarity.

CatM and BenM, which are 59% identical in sequence, both respond to the metabolite *cis,cis*-muconate (hereafter called muconate; Fig. 1) (Romero-Arroyo *et al.*, 1995; Collier *et al.*, 1998). These two LTTRs have overlapping roles in a complex regulon for aromatic compound degradation. A distinguishing characteristic of BenM is its additional ability to recognize benzoate as an inducer. At

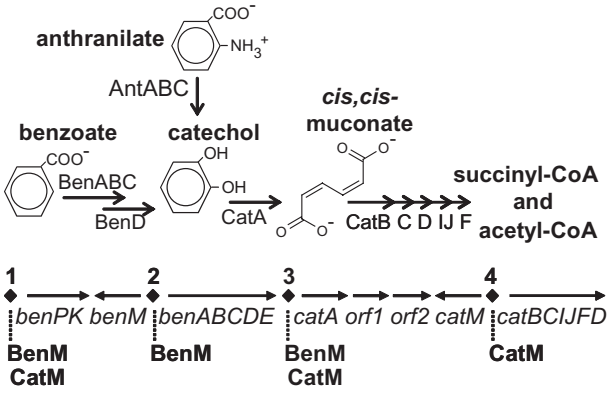

Fig. 1. Pathway for the degradation of benzoate and anthranilate. LysR-type regulators, BenM and CatM, control expression from multiple promoters (numbered 1–4) in a supraoperonic cluster of chromosomal genes. At two loci (1 and 3), BenM and CatM play equally important regulatory roles. At two loci (2 and 4), one regulator is primarily responsible for gene expression (BenM or CatM respectively). The *benPK* operon encodes transport proteins (Clark *et al.*, 2002). The *antABC* genes reside in a distant region of the chromosome and are not regulated by BenM or CatM (Bundy *et al.*, 1998).

the promoter of the *benABCDE* operon, BenM activates gene expression in response to either benzoate or muconate. When present together, the two compounds have a synergistic effect on transcriptional activation (Bundy *et al.*, 2002). This unusual type of synergism enables the bacterium to integrate multiple metabolic signals rapidly and to prevent the buildup of toxic intermediates during benzoate consumption.

Synergism may depend on changes to the electrostatic environment of muconate, housed in the primary effector-binding site, when benzoate binds the secondary site (Fig. 2; Ezezika *et al.*, 2007a; Craven *et al.*, 2008). This regulatory model derives from the analysis of BenM-EBD crystals soaked in high, non-physiological concentrations of benzoate (120 mM) (Ezezika *et al.*, 2007a). However, the structural studies do not reveal whether benzoate occupies the secondary site *in vivo* nor which interactions are critical for benzoate-dependent transcription. In the BenM-EBD structure, benzoate in the secondary site contacts arginine 160 and tyrosine 293 (Fig. 2B). Although CatM does not respond to benzoate, its comparable region is substantially conserved except for residues 160 and 293. As described herein, these amino acids in BenM were altered to prevent benzoate binding. The effects on growth and expression were used to assess how benzoate regulates transcription. Some of the resulting mutants failed to grow on benzoate, and spontaneous mutations were identified that restore this ability. Results were interpreted in light of the hypothesis that benzoate mediates transcriptional synergism by binding to the secondary site and altering interactions among charged residues at positions 160, 162 and 146 (Fig. 2).

Furthermore, arginine 156 of BenM was replaced with histidine. This variant was generated to resemble CatM(R156H), a regulator that activates transcription from the *catA* and *catB* promoters without an inducer (Neidle *et al.*, 1989; Ezezika *et al.*, 2006). This replacement, in the central portion of the EBD, is not directly adjacent to either of the structurally identified effector-binding sites. To help determine the role of this residue in mediating the response to inducers, protein structures were characterized by X-ray crystallographic methods. Here we report the structures of CatM(R156H)-EBD and BenM(R156H,T157S)-EBD and discuss conformational changes involved in transcriptional activation by LTTRs.

Results

Testing the role of R160 and Y293 of BenM in benzoate-dependent transcriptional activation

Replacements were engineered in two BenM residues predicted to mediate benzoate binding (Fig. 2B). Regulatory changes were expected to affect growth characteristics, because growth on benzoate requires BenM-

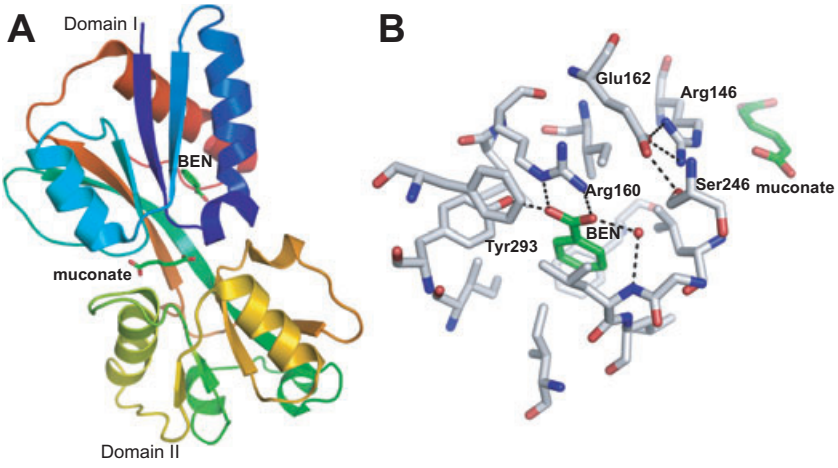

Fig. 2. Representations of the BenM-EBD structure (PDB 2F7A). A BenM-EBD subunit, in ribbon representation, shows the inducers muconate and benzoate (BEN) bound in the primary and secondary effector-binding sites respectively (A). In the region of the secondary effector-binding site, Arg160 and Tyr293 make direct contact with a bound benzoate molecule (B). A model for electrostatic control of synergism entails communication of the binding of benzoate via interactions among Arg160, Glu162 and Arg146, a residue near muconate (Ezezika *et al.*, 2007a). Residues 160 and 293 differ in CatM, which has histidine and phenylalanine at these positions respectively.

activated *ben*-gene expression (locus 2, Fig. 1) and high-level expression of the *cat*-genes. These latter genes (loci 3 and 4, Fig. 1) can be sufficiently regulated by CatM without BenM to allow growth on anthranilate or muconate. Plasmid pBAC713 (Table 1), encoding BenM(R160H,Y293F), generates a secondary effector-binding region that should resemble that of CatM, which does not respond to benzoate. DNA from pBAC713 replaced the wild-type chromosomal *benM* to generate strain ACN641 (Table 1). ACN641 was able to grow with muconate or anthranilate but not benzoate as a sole carbon source (Fig. 1). To confirm the inference that *ben*-gene expression was low, a *benA*::*lacZ* transcriptional fusion replaced *benA* on the ACN641 chromosome, generating ACN661 (Table 1). LacZ activity was measured in ACN661 and ACN32, a comparable strain with wild-type *benM* (Fig. 3). The disruption of *benA* prevents further benzoate metabolism and allows its effects as an inducer to be examined. Whereas benzoate induced a 12-fold increase in gene expression in ACN32, benzoate-dependent *benA* expression was abolished in ACN661 (Fig. 3A). In contrast, muconate increased *benA*::*lacZ* expression 18-fold in ACN661 (Fig. 3B). Although this muconate-inducible expression is lower than with wild-type BenM (ACN32), it remains higher than in the absence of BenM (ACN47) (Fig. 3B). In the latter strain, CatM mediates a low level of muconate-inducible *benA* expression (Collier *et al*., 1998). Collectively, these results indicate BenM(R160H,Y293F) activates *benA* expression in response to muconate but not benzoate. Without activation in response to benzoate, it is not surprising that the synergistic effect of both inducers, seen in ACN32, was also lost in ACN661. Interestingly, when both effectors were added to ACN661, benzoate inhibited muconate-activated *benA* expression (Fig. 3B).

Individual amino acid replacements at positions 160 and 293 in BenM

Site-directed mutagenesis was used to create BenM variants with either R160H or Y293F. Using allelic exchange methods, *benM* on the chromosome was replaced with plasmid-borne alleles. The individual amino acid replacements had similar effects to the double replacement. ACN795 and ACN824 encoding BenM(R160H) or BenM(Y293F) did not grow on benzoate. Moreover, there was no benzoate-activated *benA* expression in strains with a chromosomal *lacZ* transcriptional fusion (ACN796 and ACN826, Fig. 3A). In ACN826, the muconate-induced *benA* expression, mediated by BenM(Y293F), was strongly inhibited by benzoate (Fig. 3B). As muconate-induced *benA* expression in ACN796 was not significantly higher than in the absence of BenM (in ACN47), the BenM(R160H) protein may not be stably produced. Nevertheless, the inhibition of muconate-activated expression in ACN796 but not ACN47 may indicate that *benA* in the former strain is regulated by BenM(R160H), albeit at a low level.

To investigate position 160 in BenM further, arginine was replaced with lysine or methionine, amino acids of similar charge or size to the wild-type residue. The resulting strains, ACN810 and ACN812, which encode BenM(R160K) or BenM(R160M), respectively, failed to grow on benzoate. In the corresponding strains with a chromosomal *benA*::*lacZ* reporter (ACN811 and ACN813), gene expression indicates that both BenM variants activate transcription in response to muconate but not benzoate (Fig. 3B). However, with either replacement at residue 160, muconate-activated *benA* expression was inhibited by benzoate.

BenM(R160M,Y293F) enables growth on benzoate as a sole carbon and energy source

Additional variants were made to combine each replacement at position 160 with Y293F. When these *benM* alleles controlled *benA*::*lacZ* expression in ACN659 and ACN660, the double variants, BenM(R160M,Y293F) and BenM(R160K,Y293F), showed similar expression patterns to their single replacement counterparts (Fig. 3). However, unlike the other mutants, ACN639, encoding BenM(R160M,Y293F), grew on benzoate as the carbon source, although more slowly and with a longer lag time than the wild type (Table 2). To assess the possibility that ACN639 had acquired additional mutations, plasmid-derived *benM* DNA was used to transform a recipient encoding BenM(R160M) or BenM(Y293F). Growth on benzoate occurred only when recombination could generate an allele encoding BenM(R160M,Y293F) (data not shown). The transformation rates suggested that additional mutations are not needed for growth on benzoate.

As the BenM(R160M,Y293F) variant does not respond to benzoate (ACN659, Fig. 3A), it was not obvious how ACN639 expresses *benABCDE* sufficiently for benzoate consumption. In some mutants lacking BenM, increased levels of muconate-inducible *benA* expression permit growth on benzoate (Cosper *et al*., 2000; Ezezika *et al*., 2006). However, the muconate-dependent expression mediated by BenM(R160M,Y293F) was comparable to that of other variants that do not confer growth on benzoate (Fig. 3B). As these assays used high concentrations of extracellular effectors, conditions were modified to mimic wild-type metabolism more closely. The expression of *benA*::*lacZ* was monitored during growth on anthranilate, a substrate that generates intracellular muconate during catabolism (Fig. 1). Under these conditions, BenM(R160M,Y293F) yielded higher *benA* expression than wild-type BenM or the variants with individual

Table 1. Bacterial strains and plasmids.

Strain	Relevant characteristics[a]	Reference or source
A. baylyi strains		
ADP1	Wild-type (BD413)	Juni and Janik (1969)
ACN32	*benA*::*lacZ*-Km^r*5032*	Collier *et al.* (1998)
ACN47	*benM*::ΩS*4036 benA*::*lacZ*-Km^r*5032*	Collier *et al.* (1998)
ACN532	*benM5532* [BenM(R156H,T157S)] *benA*::*lacZ*-Km^r*5032* Δ*catMBC3205*	This study
ACN533	*benM5532* [BenM(R156H,T157S)] *benA*::*lacZ*-Km^r*5032*	This study
ACN637	*benM*::*sacB*-Km^r*5624*	This study
ACN639	*benM5639* [BenM(R160M,Y293F)]	This study
ACN640	*benM5640* [BenM(R160K,Y293F)]	This study
ACN641	*benM5641* [BenM(R160H,Y293F)]	This study
ACN659	*benM5639* [BenM(R160M,Y293F)] *benA*::*lacZ*-Km^r*5032*	This study
ACN660	*benM5640* [BenM(R160K,Y293F)] *benA*::*lacZ*-Km^r*5032*	This study
ACN661	*benM5641* [BenM(R160H,Y293F)] *benA*::*lacZ*-Km^r*5032*	This study
ACN678	*benM*5678 [BenM(R156H)]	This study
ACN680	*benM*5678 [BenM(R156H)] *benA*::*lacZ*-Km^r*5032*	This study
ACN795	*benM5795* [BenM(R160H)]	This study
ACN796	*benM5795* [BenM(R160H)] *benA*::*lacZ*-Km^r*5032*	This study
ACN807	*benM5807* [BenM(R160K,R225H,Y293F)]; spontaneous ben+ derivative of ACN640	This study
ACN809	*benM5809* [BenM(R160H,E226K,Y293F)]; spontaneous ben+ derivative of ACN641	This study
ACN810	*benM5810* [BenM(R160K)]	This study
ACN811	*benM5810* [BenM(R160K)] *benA*::*lacZ*-Km^r*5032*	This study
ACN812	*benM5812* [BenM(R160M)]	This study
ACN813	*benM5812* [BenM(R160M)] *benA*::*lacZ*-Km^r*5032*	This study
ACN824	*benM5824* [BenM(Y293F)]	This study
ACN826	*benM5824* [BenM(Y293F)] *benA*::*lacZ*-Km^r*5032*	This study
ACN828	*benM5807* [BenM(R160K,R225H,Y293F)] *benA*::*lacZ*-Km^r*5032*	This study
ACN829	*benM5809* [BenM[(R160H,E226K,Y293F)] *benA*::*lacZ*-Km^r*5032*	This study
ACN864	*benM5864* [BenM(R225H)]	This study
ACN865	*benM5864* [BenM(R225H)] *benA*::*lacZ*-Km^r*5032*	This study
ACN866	*benM5866* [BenM(E226K)]	This study
ACN867	*benM5866* [BenM(E226K)] *benA*::*lacZ*-Km^r*5032*	This study
Plasmids		
pUC19	Ap^r; cloning vector	Invitrogen
pET-21b	Ap^r; T7 promoter, expression vector	Novagen
pCR2.1-TOPO	Ap^{r}Km^r; PCR cloning vector	Invitrogen
pBAC7	Ap^r; *benKM* (563–2964)[b] region in pUC19	This study
pIB17	Ap^r; *catM3102* (11950–13205)[b] in pUC19	Neidle *et al.* (1989)
pBAC54	Ap^r Km^r; *lacZ*-Km^r cassette in NsiI site (3761)[b] in *benA* (2316–5663)[b] in pUC19	Collier *et al.* (1998)
pBAC430	Ap^r; *catM* (12116–13027)[b] in pET-21b	Bundy *et al.* (2002)
pBAC433	Ap^r; *benM* (1453–2368)[b] in pET-21b	Bundy *et al.* (2002)
pBAC668	Ap^r; *benKM* (563–2964)[b] [BenM(R156H,T157S)]	This study
pBAC680	Ap^r Km^r; PCR fragment of *catM3102* (12119–12787)[b] from PIB17 in pCR2.1-TOPO [CatM(R156H)]	This study
pBAC683	Ap^r; NdeI-XhoI 12119–12787[b] fragment from pBAC680 in pET-21b: expression construct for CatM(R156H)-EBD	This study
pBAC692	Ap^r Km^r; PCR fragment of *benM5532* (1457–2368)[b] in pCR2.1-TOPO; [BenM(R156H,T157S)]	This study
pBAC698	Ap^r; NdeI-XhoI (1457–2128)[b] fragment from pBAC692 in pET-21b; expression construct for BenM(R156H,T157S)-EBD	This study
pBAC709	Ap^r Km^r; *benKM* (563–2316)[b] pUC19. Contains *sacB*-Km^r cassette in SalI site (1930)[b] of *benM*	This study
pBAC711	Ap^r; *benM* (1453–2368)[b] [BenM(R160M,Y293F)]	This study
pBAC712	Ap^r; *benKM* (563–2964)[b] [BenM(R160K,Y293F)]	This study
pBAC713	Ap^r; *benKM* (563–2964)[b] [BenM(R160H,Y293F)]	This study
pBAC714	Ap^r; *benM* (1453–2368)[b] [BenM(R160H,Y293F)]	This study
pBAC769	Ap^r; *benM* (1453–2368)[b] [BenM(R160H)]	This study
pBAC770	Ap^r; *benM* (1453–2368)[b] [BenM(R160K)]	This study
pBAC771	Ap^r; *benM* (1453–2368)[b] [BenM(R160M)]	This study
pBAC772	Ap^r; *benM* (1453–2368)[b] [BenM(Y293F)]	This study
pBAC776	Ap^r; *benM* (1453–2368)[b] [BenM(R225H)]	This study
pBAC778	Ap^r; *benM* (1453–2368)[b] [BenM(E226K)]	This study

a. Ap^r, ampicillin resistant; Sm^r, streptomycin resistant; Sp^r, spectinomycin resistant; Km^r, kanamycin resistant; ΩS, omega cassette conferring Sm^r Sp^r (Prentki and Krisch, 1984); *sacB*, counterselectable marker, used as described previously (Jones and Williams, 2003).
b. Position in the *ben-cat* sequence in GenBank entry AF009224.

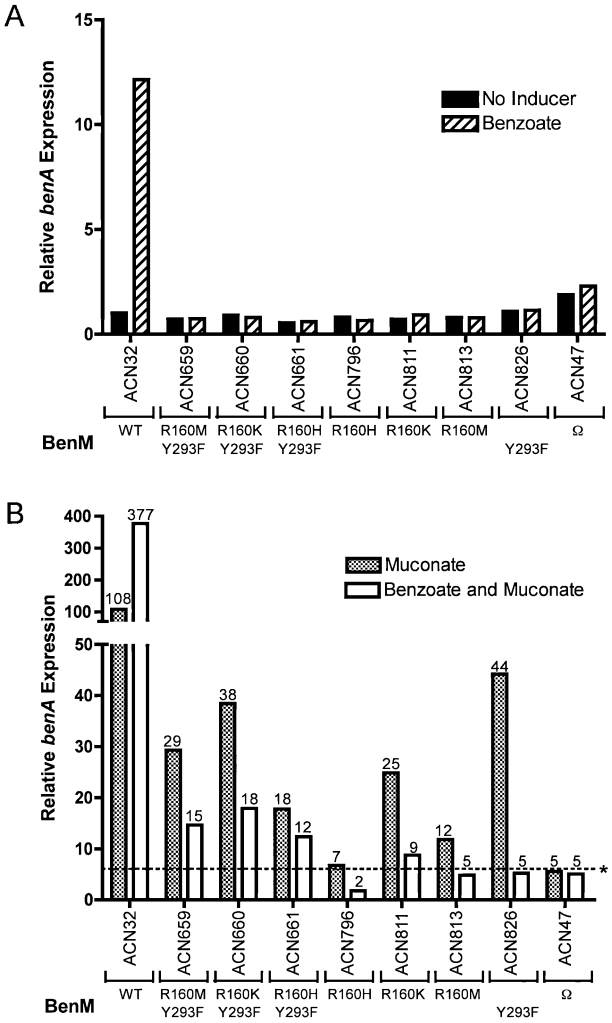

Fig. 3. Effect of *benM* alleles on expression of a chromosomal *benA*::*lacZ* transcriptional reporter. Strains and their encoded BenM variants are indicated. Controls include ACN32, with wild-type *benM* (WT), and ACN47, with an inactivated *benM* (Ω). Relative *benA* expression is reported as the ratio of measured LacZ activity to that in uninduced cultures of ACN32, 2.90 ± 0.37 (nmol/min/ml/OD_{600}). Benzoate was provided as an inducer (1 mM) (A). Muconate (1 mM) or both compounds (0.5 mM benzoate, 0.5 mM muconate) were also tested as inducers (B). The dotted line (*) represents the level of CatM-dependent *benA* expression in the presence of muconate, as observed in ACN47. All strains encode wild-type CatM. Data represent the average of four to eight replicates, and standard deviations were within 15% of the average value.

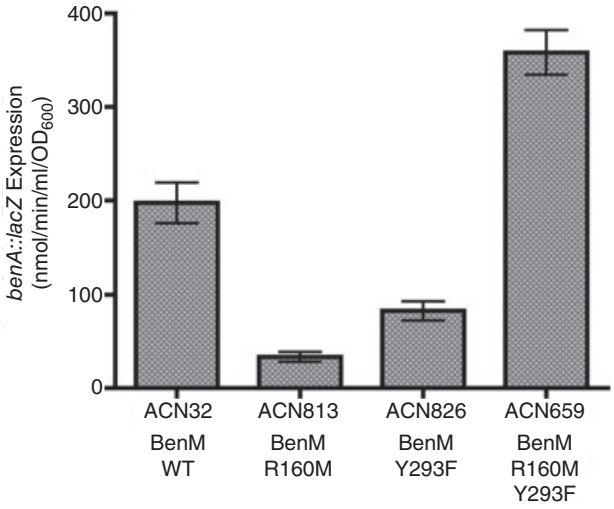

Fig. 4. Effect of *benM* alleles on *benA*::*lacZ* expression in anthranilate-grown cultures. LacZ activity was assayed early in the growth phase (OD_{600} ~0.03–0.04) for the indicated strains provided with 1 mM anthranilate as the sole carbon source. ACN32 has a wild-type (WT) BenM, and the other strains encode variants (as shown). Data represent the average of five replicates with standard deviations shown by error bars.

replacements (Fig. 4). This relatively high expression was most pronounced at early stages in the growth cycle of batch cultures (OD_{600} ~0.03–0.07). Thus, the early activation of *benA* expression by BenM(R160M,Y293F) may enable ACN639 to grow on benzoate. This variant may respond to relatively low intracellular concentrations of muconate.

Selection of spontaneous mutants that grow on benzoate (ben⁺ phenotype)

Mutants ACN640 and ACN641, which do not grow on benzoate, gave rise to spontaneous colonies on benzoate medium. Two such ben⁺ derivatives, ACN807 and ACN809, were characterized. DNA sequencing confirmed that ACN807 retained the mutations of its parent (ACN640) encoding R160K and Y293F. Similarly, ACN809 retained the mutations of its parent (ACN641) encoding R160H and Y293F. Each strain also had a *benM*

Table 2. Effect of *benM* mutations on growth with benzoate as the sole carbon source.[a]

Strain	Relevant characteristics	Generation time (min)[b]	Lag time (min)[c]
ADP1	Wild type	103 ± 5	95 ± 10
ACN639	BenM(R160M,Y293F)	147 ± 26	200 ± 30
ACN678	BenM(R156H)	83 ± 1	60 ± 5
ACN866	BenM(E226K)	85 ± 5	65 ± 5

a. Strains had comparable growth rates with succinate as the sole carbon source (data not shown).
b. Averages of at least four determinations.
c. Time between inoculation and start of exponential growth.

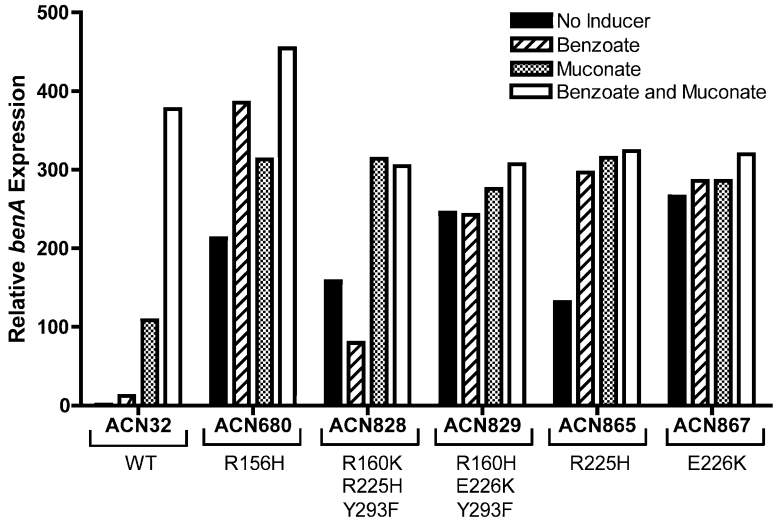

Fig. 5. Expression of a chromosomal *benA*::*lacZ* fusion in strains encoding BenM or BenM variants. Cultures were grown in LB with addition of the indicated inducer (1 mM benzoate, 1 mM muconate, or 0.5 mM benzoate and 0.5 mM muconate). β-Galactosidase activity is reported relative to uninduced ACN32 (2.90 ± 0.37 nmol/min/ml/OD_{600}). Activities are the average of at least four repetitions with standard deviations within 20% of the average value.

mutation encoding a third amino acid change, R225H in ACN807 and E226K in ACN809. Gene expression was assessed in strains with a chromosomal *benA*::*lacZ* fusion controlled by an adjacent *benM* allele encoding either BenM(R160K,R225H,Y293F) (ACN828) or BenM(R160H,E226K,Y293F) (ACN829). In both cases, there were high levels of *benA* expression, with or without the addition of muconate and/or benzoate as inducers (Fig. 5). The R225H and E226K replacements each enabled higher *benA* expression in the absence of inducer than did muconate-induced wild-type BenM.

Transcriptional activation by BenM without inducers

To determine the individual effects of R225H or E226K, engineered *benM* alleles on plasmids pBAC776 and pBAC778 were substituted for the chromosomal *benM*. Strains ACN864, encoding BenM(R225H), and ACN866, encoding BenM(E226K), grew on benzoate as the carbon source (Table 2). This ben$^+$ phenotype was consistent with having wild-type sequences in the secondary effector-binding site of BenM. Reporter strains subsequently demonstrated that the replacements at residue 225 or 226 affected gene expression. In ACN865 and ACN867, an allele encoding BenM(R225H) or BenM(E226K), respectively, controlled an adjacent chromosomal *benA*::*lacZ* fusion. Both variants activated high-level *benA* expression without added inducers (Fig. 5). The uninduced expression of *benA* in ACN867 was 266-fold higher than with wild-type BenM and was not substantially increased by benzoate or muconate. In ACN865, encoding R225H with a wild-type secondary effector-binding site, benzoate alone activated *benA* expression. In contrast, the same R225H replacement in combination with R160K and Y293F in ACN828 caused inhibition of *benA* expression when benzoate was provided as the only effector.

To improve understanding of transcriptional activation without inducers, a variant was constructed to resemble a previously studied homologue, CatM(R156H), known to induce CatA and CatB without muconate (Neidle *et al*., 1989). ACN678 was created with a chromosomal allele that encodes BenM(R156H). This strain grew well with benzoate as the carbon source (Table 2). Another strain, ACN680, was generated in which this allele controlled expression of the *benA*::*lacZ* transcriptional fusion. In the absence of inducer, *benA* expression in ACN680 under the control of BenM(R156H) was 213-fold higher than in ACN32 with wild-type BenM (Fig. 5). The addition of inducers to ACN680 elicited a further increase in gene expression.

Structural determination of CatM- and BenM-EBD R156H variant regulators

As the R156H replacement affected regulation by CatM and BenM, the variant EBD structures were characterized. In construction of the plasmid to express BenM(R156H), site-directed mutation introduced the desired replacement and an accidental change, T157S. As strains encoding BenM(R156H,T157S) regulated *benA* similarly to BenM(R156H) (data not shown), the effect of the T157S replacement was inferred to be minimal. X-ray diffraction data were collected for two independent crystal forms of BenM(R156H,T157S)-EBD without effectors. Their structures were assigned Protein Data Bank (PDB) identification codes 2H99 (crystal form A) and 2H9B (crystal Form B). Both crystallized in space group $P2_12_12_1$ with similar cell constants and were solved by molecular replacement using the co-ordinates of the previously solved BenM-EBD wild-type structure, PDB 2F7A (Ezezika *et al*., 2007a). As in previous BenM-EBD structures, two subunits related by non-crystallographic twofold symmetry

were in the asymmetric units of both crystals, although the composition of ordered ions differed between the structures. This difference in ion composition provided the impetus for comparing the two otherwise isomorphous structures. In structure 2H99, an acetate molecule bound in the primary effector-binding site of one subunit (A), while this same position in its second subunit (B) was occupied by chloride and sulphate ions. In structure 2H9B, a sulphate ion was in the primary effector-binding site of one subunit (A), while the other subunit (B) bound a sulphate and a chloride ion. Both crystal forms diffracted to high resolution (approximately 1.85 Å). Details of the data collection and refinement statistics are in Table S1 (*Supporting information*).

In contrast to BenM(R156H)-EBD, CatM(R156H)-EBD was structurally characterized only in the presence of muconate. The variant structure (PDB 3GLB) was determined using the wild-type CatM-EBD structure (PDB 2F7B) as the molecular replacement model (Ezezika *et al.*, 2007a). The CatM(R156H)-EBD structure had four subunits in the asymmetric unit (space group, $P2_12_12$) arranged as two independent dimeric units. In contrast, the previously determined CatM-EBD structures all had single subunits in the asymmetric units that could create dimers by applying crystallographic twofold operators. Muconate molecules were present in the primary effector binding sites of all the CatM(R156H)-EBD subunits. This variant crystal had a lower resolution limit of (2.8 Å) (Table S1).

Assessing structural differences

To compare the variant and wild-type EBD structures, individual subunit structures were aligned using invariant core analysis with the program Bio3D (Grant *et al.*, 2006). This analysis was consistent with the two domains of each EBD acting as rigid bodies that flex around a central hinge near residues 162 and 265. In Fig. 2A, this hinge-like region corresponds to the orange and green beta-strands depicted behind muconate. To illustrate the structural effects of the R156H replacements in BenM and CatM, residues from only domain I were aligned using invariant core analysis. The full EBD structures were then overlaid onto the aligned domain I residues. In this fashion, domain II movement could be visualized relative to a fixed domain I (Fig. 6).

To evaluate structural differences, the root mean square deviations of residues 90–161 and 267–302 of domain II were calculated between the unliganded BenM-EBD structure (2F6G, subunit A) and the other BenM-EBD structures using domain I-aligned proteins. A similar approach was used for CatM-EBD (residues 90–161 and 267–286). However, the calculated values were difficult to interpret and relatively small (with a maximum value of 1.76 Å), as reported in Tables S2 and S3. The results were complicated by the different directions of relative movement observed between domain I and domain II in different structures. Therefore, a more sophisticated method of evaluation was needed.

To improve the detection of functionally significant changes in the relative positions of the two domains of the EBDs, a domain motion analysis was performed with the program DynDom (Hayward and Berendsen, 1998; Hayward, 1999; Hayward and Lee, 2002). In this analysis, the movement of domain II with respect to a fixed domain I (containing the R156H replacement) was described by the displacement of the rigid body around a defined screw axis with a translation along this axis. Prior to the motion analysis, the individual BenM-EBD subunit structures were superimposed using core invariant residues within domain I. The CatM-EBD structures were similarly aligned and subjected to motion analysis. Domain movement can be evaluated by considering the orientation of the screw axis, as discussed later and shown in Fig. 6B and D for BenM-EBD and CatM-EBD structures respectively.

Discussion

BenM's response to benzoate requires key residues in the secondary effector-binding site

This investigation shows that benzoate-activated transcription and dual-effector synergism both depend on a BenM region distinct from the primary effector-binding site. The response to benzoate relies on two residues in a recently discovered secondary effector-binding site (Ezezika *et al.*, 2007a). Individual or double replacements of R160 and Y293 demonstrated the functional significance of this site. While these changes in BenM variants can abolish growth on benzoate and prevent benzoate-induced *benA* expression (Fig. 3A), the response to muconate was retained and appears to depend on the primary effector-binding site (Fig. 3B). Moreover, the regulatory effects of the primary and secondary effector-binding sites are interconnected (Fig. 2B). Amino acid replacements designed to prevent benzoate from binding the secondary site caused benzoate to inhibit muconate-induced *benA* expression (Fig. 3B). Without benzoate in the secondary site, there may be increased competition between benzoate and muconate to bind in the primary site. Such competition is consistent with previous effector-binding studies and the demonstration that benzoate can bind in the primary site (Clark *et al.*, 2004; Ezezika *et al.*, 2007a).

Charge-dependent interactions of residues between the primary and secondary effector-binding sites form the basis of our model for synergism (Ezezika *et al.*, 2007a; Craven *et al.*, 2008). According to this model, benzoate bound in the secondary site enhances the effect of muconate in the primary site due to interaction between

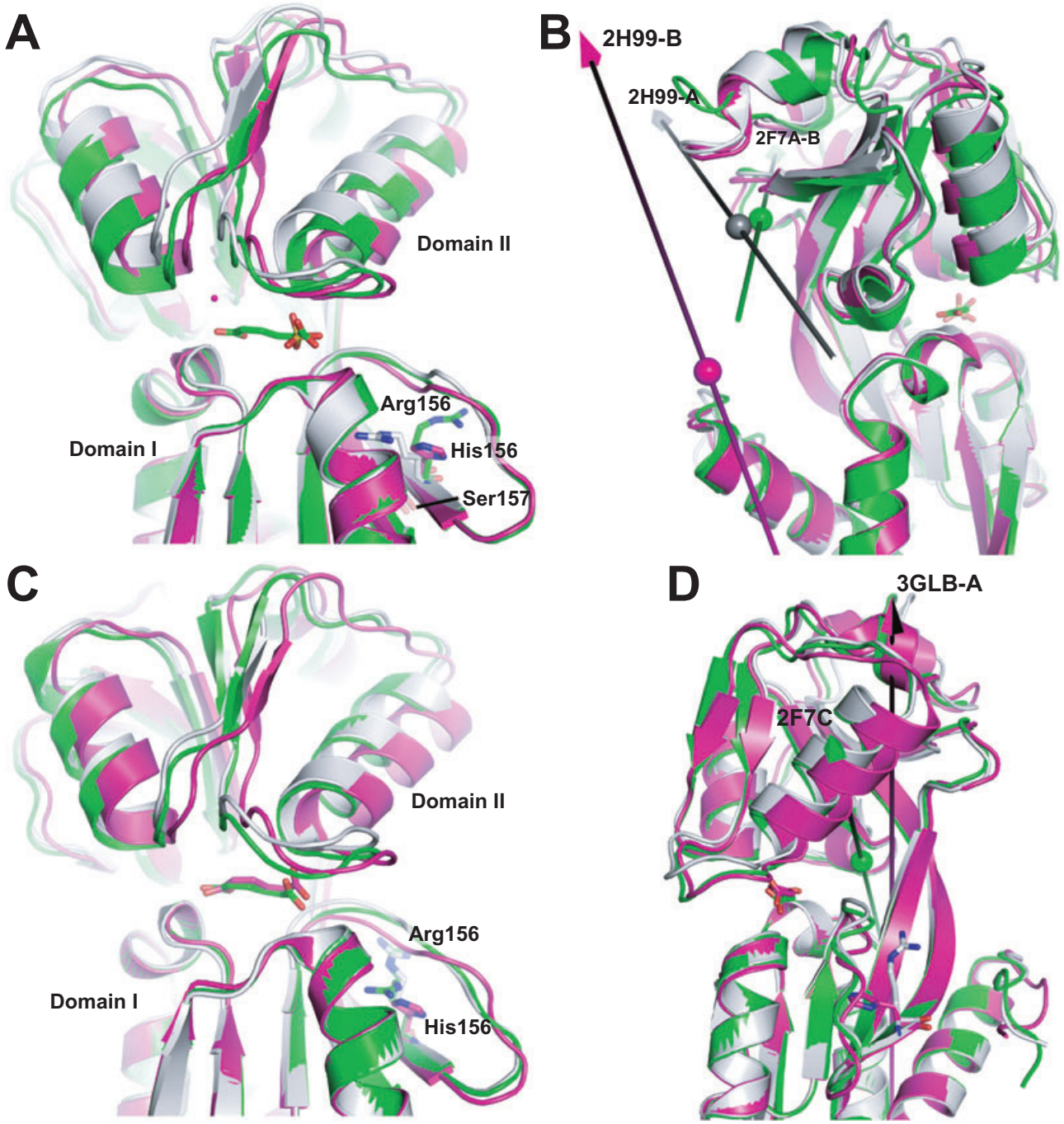

Fig. 6. Structural effects of the R156H replacement in BenM and CatM.
A. Using invariant core residues from domain I, three BenM-EBD structures were superimposed: unliganded wild type (light grey, PDB Id 2F6G subunit A), muconate-bound wild type (green, PDB Id 2F7A subunit B), and the R156H,T157S variant without effectors (magenta, PDB Id 2H99 subunit B). Chloride (magenta sphere) and sulphate ions occupy the primary effector-binding site of the variant.
B. The images from A are rotated roughly 90° about the vertical axis such that the sidelong view of muconate in the primary site becomes a head-on view. Arrows indicate the screw axes that describe the domain II motions of the BenM-EBD structures relative to the unliganded wild-type structure (2F6G, subunit A). Each axis is labelled with the Id of its structure followed by a dash and the subunit designation (A or B). Colours of the sphere and arrow point match those of the structure, except for variant 2H99-A whose structure is not shown. The two subunits of BenM(R156H,T157S)-EBD differ in the ions housed in the primary-effector binding site (Table S2).
C. A similar representation of CatM-EBD structures: unliganded wild type (light grey, PDB Id 2F7B), muconate-bound wild type (green, PDB Id 2F7C, subunit A) and muconate-bound R156H variant (magenta, PDB Id 3GLB, subunit A).
D. A rotated view of the C images showing the screw axes for CatM-EBD structures as described for B. Images depicting the screw axes for additional structures are in *Supporting information*.

the carboxyl group of benzoate and R160 (Fig. 2). This interaction decreases the attraction between R160 and E162 and enhances the opportunity for interactions between E162 and R146. This latter interaction keeps R146 from shielding the negative charge of the adjacent carboxyl group of muconate, thereby strengthening the attraction between the negatively charged effector and the positive dipole moments of four nearby alpha helices. Therefore, in the presence of benzoate, muconate should be more effective in drawing together the two domains of the EBD into an activated conformation.

The R160M and R160K replacements might be expected to affect muconate-induced gene expression differently. Without benzoate in the secondary site, methionine could enhance interaction between E162 and R146 to augment muconate induction in a fashion that mimics the benzoate-R160 contact in wild-type BenM. In contrast, the charge based attraction between K160 and E162 might resemble the effect of the R160 in the absence of benzoate, yielding lower levels of muconate-induced transcription. While R160M was not observed to enhance gene expression to a greater extent than the R160K in cultures grown with high concentrations of extracellular muconate (Fig. 3B), the only variant that allows growth on benzoate as the sole carbon source is BenM(R160M,Y293F). This result suggests that the R160M replacement is better able than R160K to activate muconate-dependent transcription *in vivo*.

Consistent with our regulatory model, R160M could enhance transcription via an increased affinity of the protein for muconate that is physiologically significant at low effector concentrations (Fig. 4). The long lag time of ACN639 suggests that growth is limited by the time needed to generate muconate as an inducer (Table 2). It is not yet clear why the Y293F replacement is also required for growth on benzoate and for the early elevation of *benA* expression (Fig. 4). Furthermore, it is not evident why the replacements at positions 160 and 293 reduced muconate-dependent *benA* expression relative to wild-type BenM (Fig. 3B). Such observations emphasize the need to investigate structural differences and protein stability in addition to correlating ongoing functional and structural analyses. A full understanding of BenM-activated expression will also require investigations of interactions with DNA and RNA polymerase, because regulation varies at different promoters. For example, BenM activates *benPK* expression (locus 1, Fig. 1) in response to muconate but not benzoate (Clark *et al*., 2002).

Transcriptional activation without effectors: the importance of protein interfaces in the tetramer

Spontaneous mutants revealed the importance of residues 225 and 226. BenM(R225H) and BenM(E226K) activated high-level *benA* expression without exogenous inducers (Fig. 5). In BenM-EBD structures, the side-chains of R225 and E226 are adjacent and lie at the centre of the dimer interface on the twofold symmetry axis (Fig. 7C). This axis, present in all our structures, is crystallographic in some cases and non-crystallographic in others. Thus, the R225H and E226K replacements are likely to affect the dimer interface. Supporting this assumption, a comparably positioned residue in CbI was shown by cross-linking studies to be required for oligomerization (Stec *et al*., 2006). Residues 225 and 226 are identified in a model of the tetrameric BenM-EBD structure (Fig. 7). Although BenM and CatM did not crystallize as tetramers, the interface between neighbouring subunits (the dimer interface) was common in all our EBD structures (Ezezika *et al*., 2007a,b). Furthermore, the organization of two BenM-EBD structures (2F8D and 2F97) in their crystal lattices mimicked a biologically active tetramer, as assessed by the remarkable similarity to tetrameric CbnR and DntR structures (Muraoka *et al*., 2003; Smirnova *et al*., 2004; Ezezika *et al*., 2007b). Mutations that cause constitutive activation in other LTTRs, such as OccR and OxyR, have also been predicted to affect the dimerization interface (Choi *et al*., 2001; Akakura and Winans, 2002). Amino acid replacements may alter the relative orientations of the subunits or the local flexibility of the protein subunits and thereby affect the function of the oligomeric protein.

The R225H replacement may favour ionic interactions between neighbouring side-chains of H225 and E125 at the expense of those with E226 (Fig. 7C). At this central location of the dimer interface, both the charge (pKa) and mass differences between arginine and histidine are likely to affect the association properties between adjacent proteins. With the E226K replacement, a hydrogen bond between K226 and E125 might pull the domains together and mimic effector-mediated activation. Without effectors, the BenM(E226K) variant activates maximal levels of transcription that are not significantly enhanced by benzoate or muconate (Fig. 5). This regulation enables ACN866 to grow rapidly on benzoate with a short lag time (Table 2).

BenM(R156H) also activates transcription without effectors and allows rapid growth on benzoate (Fig. 5, and Table 2). The importance of R156 was first found in CatM (Neidle *et al*., 1989; Ezezika *et al*., 2006). The R156H replacement, which lies at the interface between dimers (the tetramer interface), may weaken the interaction with D264 on the adjacent subunit (Fig. 7A and B). Furthermore, the R156H replacement may alter the loop of residues 148–156 and thereby impact the relationships between subunits of the oligomeric protein. The structure of the variant showed substantial repositioning of lysine at position 148 (Fig. 7B). When H156 is

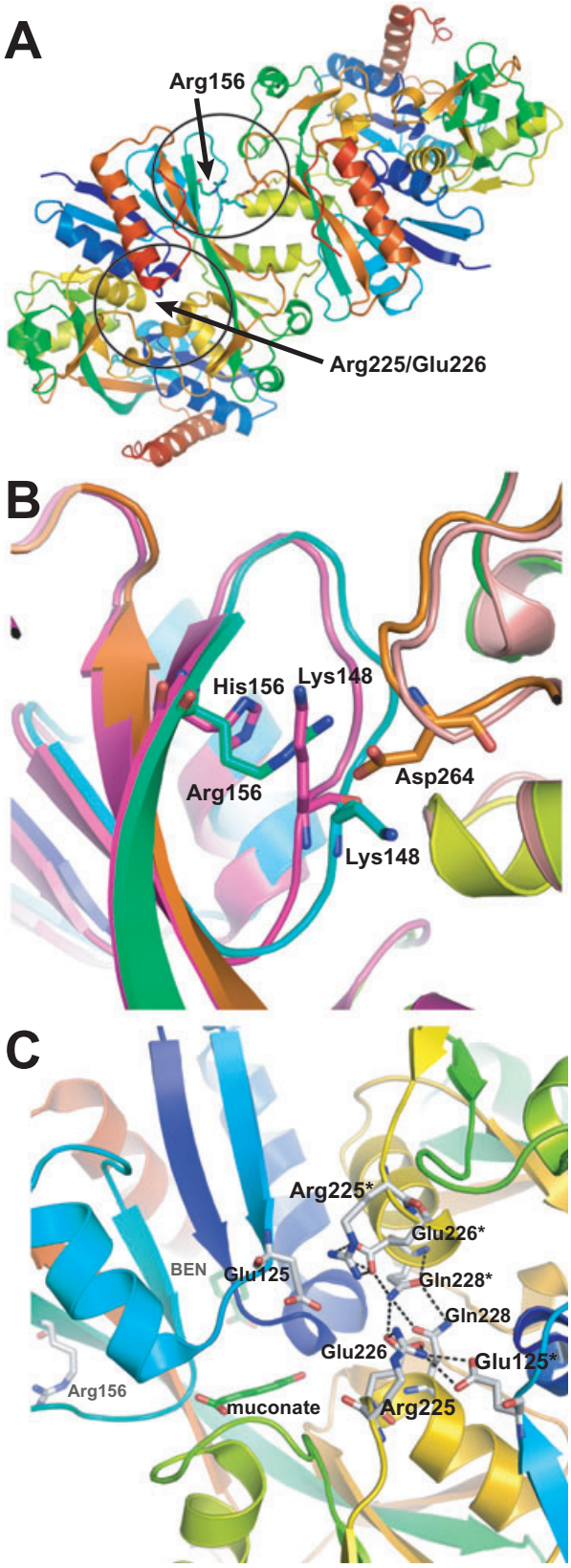

Fig. 7. Location of amino acids in BenM variants.
A. The predicted tetrameric arrangement of subunits based on the expansion of crystallographic symmetry to a BenM-EBD structure (PDB Id 2F97) (Ezezika *et al*., 2007b). Each subunit is coloured blue (N-terminus) to red (C-terminus). Circles highlight the location of variant residues.
B. An enlargement of the top circled area in A depicting the region near residue 156. The BenM(R156H,T157S)-EBD structure (PDB Id 2H99) is superimposed on that of the wild type (PDB Id 2F97) using residues within 6 Å of the interface.
C. An enlargement of the bottom circled area in A depicting the region near residues 225 and 226. Benzoate (BEN) in the secondary effector-binding site and muconate in the primary site are shown in green. Arg156 is shown for reference. Hydrogen bonds between ionic residues are depicted as dashed lines. Symmetrically related residues from the twofold-related subunit are marked with an asterisk.

present, lysine moves into the adjacent pocket normally occupied by the side-chain of arginine. Because the BenM(R156H,T127S)-EBD structures did not pack using the tetrameric interface, we cannot identify the effects on oligomer reorientation. However, as this tetrameric interface was not used for packing in the crystals, alterations in tetramer formation could not have caused the changes observed in the relative positions of the EBD domains in the wild type and the R156H variants (described next). There were fundamental changes in each subunit.

Protein conformations associated with LTTR-activated transcription and ligand binding

In LTTRs, effectors are predicted to bring the EBD domains together by binding between them (Ezezika *et al*., 2007a). Muconate in the primary site of BenM-EBD (green) resulted in a downward tilting of the right side of domain II towards domain I compared with the structure without ligands (grey, Fig. 6A). Similarly, both domains of the variant (magenta) are drawn together despite the absence of muconate (Fig. 6A). Even without the context of the functional tetramer, the variant EBD appears to assume a conformation similar to the inducer-bound wild type. As the variant contains chloride and sulphate ions in the primary effector-binding site, BenM(R156H) may activate transcription non-specifically in response to bound anions.

Structural comparisons were complex, and domain movement was not limited to rotation about a hinge. Motion analysis was used to determine the position of a screw axis to describe simultaneous rotational and translational movements of domain II given a fixed position of domain I, using the regulator without ligands as a reference (Fig. 6B). The movement of domain II towards domain I can be visualized using a right-hand rule with the thumb pointing in the direction of the arrow (translation) such that the fingers curl around in the direction of rotation.

The position of an axis representing simple rotation about an interdomain hinge is best matched by the wild-type structure with muconate and benzoate bound in the primary and secondary effector sites respectively (2F7A-B, Fig. 6B). In this inducer-bound structure, domain II rotates 5.5° with minimal translation (0.21 Å) about an axis that passes through domain II near residues 161 and 267 (Fig. 6B). The movement parameters for all our structures are given in Tables S2 and S3. The BenM(R156H,T157S)-EBD variants deviated from a perfect hinge motion to a greater extent than the inducer-bound wild-type regulator. For each variant subunit, the position of its screw axis depended on the particular ions in its primary effector-binding site (Table S2). For the structures with both chloride and sulphate ions in this site, 2H99-B (Fig. 6B) and 2H9B-B (Fig. S1), the rigid-body motion of domain II is skewed towards the location of the R156H replacement. While the significance of this twist is unknown, the R156H variants were more akin to the wild-type structure bound to muconate than to those that lacked this inducer. This conclusion is supported by assessment of the screw axis vectors and other displacement values (such as the distances between the screw axis and the line joining the centres of mass). Thus, the rigid-body motion of the domains in the BenM(R156H,T157S)-EBD variant imitated the conformational changes that typically occur upon muconate binding.

The movement analysis for CatM-EBD was more complicated. First, the wild-type structure (2F7B) contained sulphate and chloride ions in the primary effector-binding site that appeared to draw the EBD domains together in a partially closed form intermediate between the BenM-EBD structures with and without inducers (2F7A-B and 2F6G-A respectively). Second, we were only able to obtain data for muconate-bound CatM(R156H)-EBD. Nevertheless, the comparisons were informative. The EBD domains of the variant structure (magenta) were closer together when clamping down on muconate than even the inducer-bound wild type (green, Fig. 6C). As muconate-dependent induction by this R156H variant is higher than for wild-type CatM (Neidle *et al*., 1989), our data support the model that a transcriptionally active regulator has a conformation in which the two EBD domains are drawn together. Although the conformational change within each protein subunit may appear to be subtle, the propagation of small changes can result in substantial changes within the tetramer (Ezezika *et al*., 2007a).

The screw axes of the CatM(R156H)-EBD structures (3GLB, subunits A, C and D) show that relative to the wild-type structures, domain II is rotated more prevalently towards the R156H replacement (Fig. 6D and *Supporting information*). Subunit B of the CatM(R156H)-EBD structure displays the most exaggerated rotation towards the replacement (see *Supporting information*). A sulphate ion, unique to this subunit, may bridge His160 and His297 and distort the conformation. Overall, in the structures of both BenM(R156H,T157S) and CatM (R156H), the rigid-body domain motions resemble those of the muconate-bound wild-type proteins, but with a slight turn to bring domain II towards residue 156. Such a change most likely affects the relative orientations of these domains in the formation of the functional oligomeric proteins.

Dual-effector synergism and relevance to the widespread LTTR family

Although BenM is the only regulator in which distinct effector-binding sites and transcriptional synergism are known, there are likely to be related examples of multi-effector transcriptional control. A database search revealed approximately 60 BenM-like homologues in which key residues in the secondary effector-binding pocket were conserved (data not shown). Completely conserved residues included R146, R160 and E162, which may mediate transcriptional synergism, as well as R160 and Y293, which may interact with a ligand. These putative regulators also contained conserved residues in a pocket resembling the muconate-binding primary effector-binding site of BenM and CatM. These homologues were identified in diverse bacteria including different species of *Burholderia*, *Ralstonia*, *Psychrobacter*, *Polaromonas*, *Methylobacterium*, *Sphingomonas*, *Bordatella*, *Xanthobacter*, *Paracoccus* and *Acinetobacter*.

The study of a BenM homologue from *Acinetobacter calcoaceticus* PHEA2, 84% identical to that of ADP1, did not identify synergism (Zhan *et al*., 2008). However, this investigation did not assess the uptake of compounds added as inducers or whether they were metabolized. Thus, some questions remain about these conclusions. The effector responses of many LTTRs involved in aromatic compound degradation have proven difficult to study. Nevertheless, the potential use of such regulators for purposes such as biosensing and bioengineering are driving efforts to create regulators with increased sensitivity to specific inducers and/or more varied effector-binding profiles (Cebolla *et al*., 1997; 2001; Smirnova *et al*., 2004; Lonneborg *et al*., 2007). Our structure-function studies of BenM and CatM may be helpful in extending such biotechnology applications for the LTTR family.

Experimental procedures

Bacterial strains and growth conditions

Acinetobacter baylyi strains (Table 1) and *Escherichia coli* were grown in Luria–Bertani (LB) broth at 37°C with shaking

(300 r.p.m.) (Sambrook *et al.*, 1989). Alternatively, *A. baylyi* was grown in minimal medium with succinate (10 mM), anthranilate (2 mM), benzoate (2 mM), or muconate (2 mM) as the carbon source (Shanley *et al.*, 1986). *E. coli* DH5α (Invitrogen) and XL1-Blue (Stratagene) were used as plasmid hosts. Antibiotics were added, as needed, to the following concentrations: ampicillin, 150 μg ml^{-1}; kanamycin, 25 μg ml^{-1}; streptomycin, 13 μg ml^{-1}; spectinomycin, 13 μg ml^{-1}. For *A. baylyi* growth curves, succinate-grown colonies were used to inoculate 5 ml cultures. After overnight growth on benzoate, 1 ml was used to inoculate 100 ml of benzoate medium. Growth was assessed by turbidity and measured spectrophotometrically (OD_{600}).

Site-specific mutagenesis of benM *and generation of* A. baylyi *strains via allelic exchange*

Site-directed mutagenesis of plasmid-borne *benM* (QuikChange, Stratagene) was used to encode desired amino acids. Template plasmids, pBAC7 or pBAC433, were used in PCR reactions with mutagenic primers (Table S4). DpnI-treated PCR products were transformed into XL1-Blue cells, and plasmid-containing colonies were selected. DNA sequencing confirmed nucleotide substitutions on plasmids. Plasmid-borne alleles were used to replace chromosomal genes (Collier *et al.*, 1998). To aid the introduction of altered *benM* DNA, a counter-selectable marker disrupted chromosomal *benM*. Plasmid pBAC709 was made by ligating the ~3.65 kb *sacB*::Km^r cassette from PRMJ1 (Jones and Williams, 2003) into the SalI site of *benM* on pBAC11. pBAC709 was linearized with AlwN1 and used to transform ADP1, generating ACN637. To replace the chromosomal *sacB* marker with modified *benM* alleles, appropriate plasmids were linearized with XhoI or PvuII and used to transform ACN637. Desired transformants were selected by growth at 30°C in the presence of 5% sucrose. In resulting strains, the chromosomal *benM* was PCR amplified and confirmed by DNA sequencing.

β-Galactosidase assays to measure benA::lacZ *expression*

A *benA*::*lacZ* transcriptional fusion was introduced into the chromosome of *A. baylyi* strains by allelic exchange with DNA from pBAC54 linearized with XmnI. Unless otherwise noted, strains were grown overnight in LB with kanamycin. The following day, strains were subcultured into LB with no inducer or the following: benzoate (1 mM), muconate (1 mM) or both (0.5 mM each). Cell density was measured at 600 nm, and LacZ activity was assayed when cultures entered stationary phase (Miller, 1972). Using the FlourAce β-galactosidase reporter kit (Bio-Rad), the hydrolysis of 4-methylumbelliferyl-galactopyranoside to the product 4-methylumbelliferone was detected with a TD-360 minifluorometer. For assays during growth on anthranilate, cultures were first grown overnight in 5 ml LB with kanamycin. The following morning, 100 μl of each culture was diluted into 5 ml of minimal medium with 1 mM anthranilate as the sole carbon source. LacZ activity was measured at specific times following inoculation.

Transformation assay used to confirm the ben+ growth phenotype of ACN639

To assess the ben$^+$ phenotype of ACN639, transformation assays were performed. ACN824, encoding the Y293F replacement, was used as the recipient with donor DNA from plasmids. pBAC711, pBAC771 and pBAC772 were linearized by digestion with XhoI, and pBAC780 with EcoRI, before being used to transform ACN824 (Table 1). The same transformations were done using ACN812, encoding BenM(R160M), as the recipient strain. Transformants grew on benzoate only when an allele could be generated to encode BenM(R160M,Y293F).

Expression and purification of BenM- and CatM-EBD variants

The EBDs of BenM(R156H,T157S) and CatM(R156H) were purified from *E. coli* BL21(DE3) Gold cells (Stratagene) harbouring expression plasmids pBAC698 or pBAC683 respectively. For expression, *E. coli* cultures were grown at 37°C to an OD_{600} of ~0.2 at which time isopropyl-β-D-thiogalactopyranoside (0.2 mM) was added for induction. Cells were harvested after overnight growth and suspended in lysis buffer (20 mM Tris-HCl, 500 mM NaCl, 10% [v/v] glycerol, 5 mM imidazole, pH 7.9) at 4°C. Cells were lysed by French Press (15 000 psi) at 4°C. The cell lysate was centrifuged at 15 000 *g* for 15 min at 4°C and the clarified cell extract was applied to a Hi-Trap 5 ml metal chelating column (GE Biosciences) charged with nickel. Purified BenM(R156H,T157S)-EBD samples were dialysed twice against 20 mM Tris-HCl (pH 7.9), 500 mM NaCl, 10% (v/v) glycerol and concentrated to ~14 mg ml^{-1}. Purified CatM(R156H)-EBD was dialysed against 20 mM Tris-HCl, 250 mM imidazole (pH 7.9), 500 mM NaCl, 10% (v/v) glycerol. Imidazole and glycerol were added to increase protein solubility.

Crystallization and X-ray analyses

Initial high-throughput crystallization screens at the Hauptman-Woodward Institute used microbatch under oil methods at 298K (Luft *et al.*, 2001). Screens were done with and without benzoate and/or muconate (100 mM) in the protein solution. Conditions yielding crystals were optimized in-house with the microbatch under oil method at 15°C or 25°C with 2 μl protein and 2 μl precipitant. Two conditions produced BenM(R156H,T157S)-EBD crystals. Crystal Form A came from a precipitant solution of 0.015 M magnesium acetate, 0.05 M sodium cacodylate, 1.7 M ammonium sulphate, pH 6.0; and Crystal Form B was derived from 2.0 M ammonium sulphate as precipitant. CatM(R156H) crystals grew from a precipitant of 1.6 M ammonium sulphate, 0.1 M citric acid, pH 4.0 with 100 mM muconate (from a 500 mM, pH 7.0 stock solution). Protein samples were centrifuged for 5 min at 16 000 *g* and allowed to equilibrate to room temperature before crystallization trials. Crystals for X-ray diffraction studies grew within 1–2 weeks.

Diffraction data for BenM(R156H,T157S)- and CatM(R156H)-EBD were collected at the South-east Regional Collaborative Access Team (SER-CAT) at the 22-ID

and 22-BM beamlines at the Advanced Photon Source, Argonne, Il with 0.5° oscillations and wavelength of 1.0 Å. Data were processed with beamline versions of HKL2000 (Otwinowski and Minor, 1997). Structures were determined as before (Ezezika *et al*., 2007a,b) by molecular replacement using MOLREP in the CCP4 suite (1994) with known EBD co-ordinates (PDB accession 2F6G and 2F7A for the BenM variant and 2F7B and 2F7C for the CatM variant) as search models. COOT (Emsley and Cowtan, 2004) was used to adjust local differences in the structures, and atomic refinement performed with REFMAC (Murshudov *et al*., 1997). Refinement of the four non-crystallographically related subunits of CatM(R156H) used medium NCS restraints on four groups defined by residues 90–155, 157–219, 221–275 and 277–296. Residues 297–307 at the C-termini were ordered to different degrees in each subunit and assumed several conformations. Data collection and refinement statistics are in *Supporting information*.

Invariant core residues were identified and aligned in the program Bio3d (Grant *et al*., 2006) with a 0.5 $Å^3$ core cut-off. Atomic co-ordinates were aligned with different combinations of structures and subsets: full EBD subunits, domain I alone, domain II alone (residues), and as separate homologues or together. The overall root mean square (rms) deviations of the domain I residues were small (~0.6–1.2 Å) and not substantially increased in the local regions of the replacements in variant structures. For graphical representations, BenM-EBDs were aligned on core residues from domain I (91–98, 100–109, 111–112, 121–127, 130–146, 154–60,268–274 and 281–293). CatM-EBDs were aligned on core residues (91–123, 125, 127–146, 154–154, 156–161, 268–274, 277–277, 279–293 and 295–295). The molecular graphics program PYMOL (DeLano, 2002) was used for visualization, figure preparation and rms calculations of aligned molecules.

Domain motions were evaluated using the Domain Select option of web-based Protein Domain Motion Analysis program DynDom (Hayward and Berendsen, 1998; Hayward and Lee, 2002). For domain analysis, the pre-aligned subunits from invariant core analysis were truncated at the N- (residue 90) and C-termini (residue 302 for BenM, residue 296 for CatM), alternative side-chain conformations were removed, and the subunits were entered with domain I as the fixed domain (for BenM, residues 90–161 and 267–302; for CatM, residues 90–161 and 267–286) and domain II (residues 162–266) as the moving domain. Screw axes were visualized as CGI objects by reformatting the Rasmol (Sayle and Milner-White, 1995) output of the DynDom program for visualization in the program PYMOL (DeLano, 2002). Screw axis vectors and centre points were similarly calculated using a python script with data from the Rasmol output.

Acknowledgements

We thank Jennifer Hiras and Samantha Zelin, both supported by NSF Research Experience for Undergraduates grant DBI-0453353, for assisting with strain construction. We are grateful to the staff at the Hauptman-Woodward Institute for performing the high-throughput crystallization screens, to Dr Santiago Lima for assistance in crystallographic data collection and structure determination, and the staffs at the SBC-CAT and SER-CAT beamlines for assistance in X-ray data collection and the use of their facilities. Use of the Advanced Photon Source was supported by the US Department of Energy, Office of Science, and Office of Basic Energy Sciences under Contract No. W-31–109-Eng-38. The research was funded by National Science Foundation Grants MCB-0346422 (to C.M.) and MCB-0516914 (to E.L.N.).

References

Collaborative Computational Project, Number 4 (1994) The CCP4 suite: programs for protein crystallography. *Acta Crystallogr D Biol Crystallogr* **50:** 760–763.

Akakura, R., and Winans, S.C. (2002) Constitutive mutations of the OccR regulatory protein affect DNA bending in response to metabolites released from plant tumors. *J Biol Chem* **277:** 5866–5874.

Bundy, B.M., Campbell, A.L., and Neidle, E.L. (1998) Similarities between the *antABC*-encoded anthranilate dioxygenase and the *benABC*-encoded benzoate dioxygenase of *Acinetobacter* sp. strain ADP1. *J Bacteriol* **180:** 4466–4474.

Bundy, B.M., Collier, L.S., Hoover, T.R., and Neidle, E.L. (2002) Synergistic transcriptional activation by one regulatory protein in response to two metabolites. *Proc Natl Acad Sci USA* **99:** 7693–7698.

Cebolla, A., Sousa, C., and de Lorenzo, V. (1997) Effector specificity mutants of the transcriptional activator NahR of naphthalene degrading *Pseudomonas* define protein sites involved in binding of aromatic inducers. *J Biol Chem* **272:** 3986–3992.

Cebolla, A., Sousa, C., and de Lorenzo, V. (2001) Rational design of a bacterial transcriptional cascade for amplifying gene expression capacity. *Nucleic Acids Res* **29:** 759–766.

Choi, H., Kim, S., Mukhopadhyay, P., Cho, S., Woo, J., Storz, G., and Ryu, S. (2001) Structural basis of the redox switch in the OxyR transcription factor. *Cell* **105:** 103–113.

Clark, T.J., Momany, C., and Neidle, E.L. (2002) The *benPK* operon, proposed to play a role in transport, is part of a regulon for benzoate catabolism in *Acinetobacter* sp. strain ADP1. *Microbiology* **148:** 1213–1223.

Clark, T.J., Phillips, R.S., Bundy, B.M., Momany, C., and Neidle, E.L. (2004) Benzoate decreases the binding of *cis,cis*-muconate to the BenM regulator despite the synergistic effect of both compounds on transcriptional activation. *J Bacteriol* **186:** 1200–1204.

Collier, L.S., Gaines, G.L., 3rd, and Neidle, E.L. (1998) Regulation of benzoate degradation in *Acinetobacter* sp. strain ADP1 by BenM, a LysR-type transcriptional activator. *J Bacteriol* **180:** 2493–2501.

Cosper, N.J., Collier, L.S., Clark, T.J., Scott, R.A., and Neidle, E.L. (2000) Mutations in *catB*, the gene encoding muconate cycloisomerase, activate transcription of the distal *ben* genes and contribute to a complex regulatory circuit in *Acinetobacter* sp. strain ADP1. *J Bacteriol* **182:** 7044–7052.

Craven, S.H., Ezezika, O.C., Momany, C. and Neidle, E.L. (2008) LysR homologs in *Acinetobacter*: insights into a diverse and prevalent family of transcriptional regulators. In *Acinetobacter Molecular Biology*. Gerischer, U. (ed.). Norfolk: Caister Academic Press, pp. 163–202.

DeLano, W.L. (2002) *The Pymol User's Manual*. San Carlos, CA: DeLano Scientific.

Emsley, P., and Cowtan, K. (2004) Coot: model-building tools for molecular graphics. *Acta Crystallogr D Biol Crystallogr* **60:** 2126–2132.

Ezezika, O.C., Collier-Hyams, L.S., Dale, H.A., Burk, A.C., and Neidle, E.L. (2006) CatM regulation of the *benABCDE* operon: functional divergence of two LysR-type paralogs in *Acinetobacter baylyi* ADP1. *Appl Environ Microbiol* **72:** 1749–1758.

Ezezika, O.C., Haddad, S., Clark, T.J., Neidle, E.L., and Momany, C. (2007a) Distinct effector-binding sites enable synergistic transcriptional activation by BenM, a LysR-type regulator. *J Mol Biol* **367:** 616–629.

Ezezika, O.C., Haddad, S., Neidle, E.L., and Momany, C. (2007b) Oligomerization of BenM, a LysR-type transcriptional regulator: structural basis for the aggregation of proteins in this family. *Acta Crystallogr Sect F Struct Biol Cryst Commun* **63:** 361–368.

Grant, B.J., Rodrigues, A.P., Sawy, K.M.E.I., McCammon, J.A., and Caves, L.S. (2006) Bio3d: an R package for the comparative analysis of protein structures. *Bioinformatics* **22:** 2695–2696.

Hayward, S. (1999) Structural principles governing domain motions in proteins. *Proteins* **36:** 425–435.

Hayward, S., and Berendsen, H.J. (1998) Systematic analysis of domain motions in proteins from conformational change: new results on citrate synthase and T4 lysozyme. *Proteins* **30:** 144–154.

Hayward, S., and Lee, R.A. (2002) Improvements in the analysis of domain motions in proteins from conformational change: DynDom version 1.50. *J Mol Graph Model* **21:** 181–183.

Jones, R.M., and Williams, P.A. (2003) Mutational analysis of the critical bases involved in activation of the AreR-regulated sigma54-dependent promoter in *Acinetobacter* sp. strain ADP1. *Appl Environ Microbiol* **69:** 5627–5635.

Juni, E., and Janik, A. (1969) Transformation of *Acinetobacter calco-aceticus* (*Bacterium anitratum*). *J Bacteriol* **98:** 281–288.

Lonneborg, R., Smirnova, I., Dian, C., Leonard, G.A., and Brzezinski, P. (2007) *In vivo* and *in vitro* investigation of transcriptional regulation by DntR. *J Mol Biol* **372:** 571–582.

Luft, J.R., Wofley, J., Jusrisica, I., Glasgow, J., Fortier, S., and DeTitta, G.T. (2001) Macromolecular crystallization in a high throughput laboratory- the search phase. *J Crystal Growth* **232:** 591–595.

Miller, J.H. (1972) *Experiments in Molecular Genetics*. Cold Spring Harbor, NY: Cold Spring Harbor Laboratory.

Muraoka, S., Okumura, R., Ogawa, N., Nonaka, T., Miyashita, K., and Senda, T. (2003) Crystal structure of a full-length LysR-type transcriptional regulator, CbnR: unusual combination of two subunit forms and molecular bases for causing and changing DNA bend. *J Mol Biol* **328:** 555–566.

Murshudov, G.N., Vagin, A.A., and Dodson, E.J. (1997) Refinement of macromolecular structures by the maximum-likelihood method. *Acta Crystallogr D Biol Crystallogr* **53:** 240–255.

Neidle, E.L., Hartnett, C., and Ornston, L.N. (1989) Characterization of *Acinetobacter calcoaceticus catM*, a repressor gene homologous in sequence to transcriptional activator genes. *J Bacteriol* **171:** 5410–5421.

Otwinowski, Z., and Minor, W. (1997) Processing of X-ray diffraction data collected in oscillation mode. *Methods Enzymol* **276:** 307–326.

Pareja, E., Pareja-Tobes, P., Manrique, M., Pareja-Tobes, E., Bonal, J., and Tobes, R. (2006) ExtraTrain: a database of extragenic regions and transcriptional information in prokaryotic organisms. *BMC Microbiol* **6:** 29.

Prentki, P., and Krisch, H.M. (1984) *In vitro* insertional mutagenesis with a selectable DNA fragment. *Gene* **29:** 303–313.

Quiocho, F.A., and Ledvina, P.S. (1996) Atomic structure and specificity of bacterial periplasmic receptors for active transport and chemotaxis: variation of common themes. *Mol Microbiol* **20:** 17–25.

Romero-Arroyo, C.E., Schell, M.A., Gaines, G.L., 3rd, and Neidle, E.L. (1995) catM encodes a LysR-type transcriptional activator regulating catechol degradation in *Acinetobacter calcoaceticus*. *J Bacteriol* **177:** 5891–5898.

Sambrook, J., Fritsch, E.F., and Maniatis, T. (1989) *Molecular Cloning: A Laboratory Manual*, 2nd edn. Cold Spring Harbor, NY: Cold Spring. Harbor Laboratory Press.

Sayle, R.A., and Milner-White, E.J. (1995) RASMOL: biomolecular graphics for all. *Trends Biochem Sci* **20:** 374.

Shanley, M.S., Neidle, E.L., Parales, R.E., and Ornston, L.N. (1986) Cloning and expression of *Acinetobacter calcoaceticus catBCDE* genes in *Pseudomonas putida* and *Escherichia coli*. *J Bacteriol* **165:** 557–563.

Smirnova, I.A., Dian, C., Leonard, G.A., McSweeney, S., Birse, D., and Brzezinski, P. (2004) Development of a bacterial biosensor for nitrotoluenes: the crystal structure of the transcriptional regulator DntR. *J Mol Biol* **340:** 405–418.

Stec, E., Witkowska-Zimny, M., Hryniewicz, M.M., Neumann, P., Wilkinson, A.J., Brzozowski, A.M. *et al.* (2006) Structural basis of the sulphate starvation response in *E. coli*: crystal structure and mutational analysis of the cofactor-binding domain of the Cbl transcriptional regulator. *J Mol Biol* **364:** 309–322.

Tyrrell, R., Verschueren, K.H., Dodson, E.J., Murshudov, G.N., Addy, C., and Wilkinson, A.J. (1997) The structure of the cofactor-binding fragment of the LysR family member, CysB: a familiar fold with a surprising subunit arrangement. *Structure* **5:** 1017–1032.

Verschueren, K.H., Tyrrell, R., Murshudov, G.N., Dodson, E.J., and Wilkinson, A.J. (1999) Solution of the structure of the cofactor-binding fragment of CysB: a struggle against non-isomorphism. *Acta Crystallogr D Biol Crystallogr* **55:** 369–378.

Zhan, Y., Yan, H., Yu, Y., Chen, M., Lu, W., Li, S., Peng, Z. *et al.* (2008) Genes involved in the benzoate catabolic pathway in *Acinetobacter calcoaceticus* PHEA-2. *Curr Microbiol* **57:** 609–614.

Supporting information

Additional supporting information may be found in the online version of this article.

Please note: Wiley-Blackwell are not responsible for the content or functionality of any supporting materials supplied by the authors. Any queries (other than missing material) should be directed to the corresponding author for the article.

